

# Sparse Latent Factor Forecaster (SLFF) with Iterative Inference for Transparent Multi-Horizon Commodity Futures Prediction

Abhijit Gupta, PhD



[abhijit.gupta\\_in@outlook.com](mailto:abhijit.gupta_in@outlook.com)

## TITLE PAGE

**Manuscript Title:**

Sparse Latent Factor Forecaster (SLFF) with Iterative Inference for Transparent Multi-Horizon Commodity Futures Prediction

**Manuscript Type:**

Research Article

**Author:**

Abhijit Gupta, PhD

Affiliation: Independent Researcher

ORCID: 0000-0002-6292-3789

Email: [abhijit.gupta\\_in@outlook.com](mailto:abhijit.gupta_in@outlook.com)

**Corresponding Author:**

Abhijit Gupta, PhD (email above)

**Running Title (suggested):**

SLFF for Commodity Futures Forecasting

**Keywords (suggested):**

commodity forecasting; multi-horizon prediction; latent factors; interpretability; time series; deep learning

**Word Count (approx., excluding references):**

7204

**Figures:**

4

**Tables:**

16

**Funding:**

None

**Competing Interests:**

None

**Ethics Approval:**

Not applicable (no human or animal subjects).

**Data Availability:**

See the manuscript Data Availability and Licensing section. The study uses a mix of public and proprietary sources; proprietary datasets require the corresponding licenses.

**Permissions to Reproduce Material:**

All figures and tables are original. Underlying data include public and proprietary sources; permissions/licenses are as described in the Data Availability section.

## Abstract

Commodity futures are volatile. Forecasting across horizons with interpretable drivers remains challenging. We propose the **Sparse Latent Factor Forecaster with Iterative Inference (SLFF)**, a structured-prediction latent-variable model that combines sparse coding, unrolled optimization, and amortized inference. SLFF explicitly optimizes a sparse latent code to explain multi-horizon futures trajectories and trains an encoder whose outputs are validated against the optimization-based solution before deployment. The method is paired with an information-set-aware pipeline (vintage macro releases, lag-aware fills, leakage checks) and evaluated under rolling-origin folds against representative statistical and neural baselines. We provide quantitative criteria for factor labeling and directional diagnostics that account for no-change regimes. On Copper and WTI futures (2005–2023), SLFF achieves competitive RMSE/MAE, improves directional skill beyond persistence, and yields factors that are stable across seeds and linked to measurable fundamentals. Code, diagnostics, and information-set specifications are released for reproducibility.

# 1 Introduction

Commodity markets, and their associated futures contracts, form a critical part of the global economy, providing essential raw materials and hedging instruments. The prices of key commodity futures, such as those for industrial metals like Copper and energy benchmarks like Crude Oil, are not merely transactional figures; they are vital indicators of economic health, drivers of industrial costs, and significant factors influencing inflation, trade balances, and geopolitical dynamics. Copper futures, for instance, are closely watched for signals about global industrial demand. Crude Oil futures are pivotal for managing energy price risk and reflect complex geopolitical and supply/demand interactions.

The inherent volatility of these commodity futures prices presents substantial risks and opportunities for a wide spectrum of market participants. Producers and consumers use futures to hedge price uncertainty, while financial institutions and traders engage in speculative and arbitrage activities. Consequently, the ability to accurately forecast commodity futures prices across various time horizons is of paramount importance for effective risk mitigation, optimized resource allocation, and informed investment decisions.

The challenge lies in the sheer complexity of factors driving futures prices. These markets are influenced by a confluence of interconnected forces:

1. **Macroeconomic Environment:** Global GDP growth, industrial production, interest rates, currency exchange rates (particularly the US Dollar), and inflation expectations.
2. **Underlying Physical Market Fundamentals:** For Copper, this includes mine production, scrap availability, and inventory levels. For Crude Oil, factors include OPEC+ decisions, non-OPEC output, geopolitical events in producing regions, and inventory levels.
3. **Demand Fundamentals:** Linked to manufacturing activity, construction, transportation needs, and energy transition dynamics.
4. **Market Sentiment and Financialization:** Speculative positioning in futures and options markets (e.g., CFTC Commitment of Traders reports), algorithmic trading, and broader risk-on/risk-off sentiment.
5. **Other factors:** Including weather patterns impacting supply/demand and inter-commodity relationships.

This intricate web of high-dimensional, often collinear, and dynamically interacting drivers makes futures price forecasting an exceptionally challenging task, characterized by non-linear relationships and regime shifts. Existing approaches often face a trade-off between predictive accuracy and interpretability. Classical time series models (ARIMA, GARCH) may struggle with non-linearities and exogenous factors. Econometric structural models rely on strong assumptions. While traditional machine learning (SVM, Random Forests) and standard deep learning models (LSTMs, CNNs) can capture complex patterns, they often function as "black boxes," limiting actionable insights [41]. There is a need for models that not only forecast accurately but also provide an understanding of the underlying drivers.

Given these limitations, this research addresses the question: *How can we develop a latent-variable forecasting framework that remains faithful to the information set, attains robust multi-horizon accuracy, and exposes stable economic factors?* We answer with the **Sparse Latent Factor Forecaster with Iterative Inference (SLFF)**, a structured-prediction model that uses an explicit latent-factor optimization layer together with a LISTA-style amortized encoder [34]. The latent code  $\mathbf{z}$  is never treated as a reconstruction target; it is the solution of a constrained regression problem that explains future trajectories under an L1 sparsity prior.

This paper makes the following contributions:

1. **Method:** We introduce SLFF, a sparse latent-factor forecaster with iterative inference, and describe a latent inference objective that supports both test-time amortization and (optionally) unrolled, differentiable optimization.
2. **Information set:** We specify an information-set-aware data pipeline, including release calendars and vintage macroeconomic series (ALFRED/FRED-MD, IMF WEO vintages), and provide an “available-at- $t$ ” specification to prevent mixed-frequency leakage.
3. **Evaluation:** We evaluate on six rolling-origin folds (train: 6y, val: 1y, test: 1y) with test years spanning 2013–2023 (every two years), reporting mean  $\pm$  standard deviation across folds and random seeds.
4. **Baselines:** We compare against PatchTST, Temporal Fusion Transformer (TFT), N-HiTS, DeepAR, and tuned gradient boosting models under matched hyperparameter budgets and learning-rate schedules.
5. **Ablations:** We present ablations over sparsity, iterative inference, latent dimensionality, and training regimes to quantify their impact on deployed forecasting accuracy and latent interpretability.
6. **Directional diagnostics:** We report directional metrics that account for no-change regimes (no-change rate, class-conditional hit rates, MCC, calibration curves, confusion matrices).
7. **Factor validation:** We evaluate factor stability via Procrustes alignment across random seeds and validate factors against observable disruption/event indicators, including counterfactual perturbation tests.
8. **Reproducibility:** We provide code (JAX/Flax), experiment manifests, Dockerized data pipelines, compute footprints, and an executable feature notebook to support replication and extension.

The remainder of this paper revisits the related work, describes SLFF in detail, specifies the curated information set, explains the experimental protocol, and presents empirical/interpretability evidence before concluding with limitations and future work.

## 2 Review of Related Work in Commodity Forecasting

### 2.1 Introduction to Commodity Price Forecasting: Significance and Challenges

Accurate forecasting of commodity prices is crucial, given their extensive impact on economies and daily life [1]. Variations in prices of essential goods affect economic activities and individual well-being [30]. Macroeconomic stability of commodity-dependent countries is closely linked to price fluctuations [15], and predicting staple commodity prices is vital for food security [29]. Reliable forecasts are essential for producers, traders, investors, and policymakers.

Commodity price forecasting is notably challenging due to inherent market complexity, volatility, nonlinear relationships, and nonstationary trends [37]. Prices respond to numerous interrelated factors including supply/demand fundamentals, macroeconomic indicators, financial market influences, geopolitical events, and environmental variables. These factors evolve, with increased financialization, global crises, and climate change adding unpredictability, often rendering traditional methods inadequate.

### 2.2 Traditional Econometric Approaches: Foundations and Limitations

Quantitative commodity forecasting historically relied on models like ARIMA, VAR, and VECM. Box-Jenkins ARIMA models [11] gained popularity for their statistical properties [64]. GARCH models [10, 27] were developed to address time-varying volatility. However, these models struggle with the nonlinearities and structural breaks common in commodity prices [84, 73], often underperforming [9]. Their limitations spurred exploration of more flexible paradigms [75, 52].

### 2.3 Rise of Machine Learning in Commodity Forecasting

ML and AI techniques have become prominent alternatives [16, 80]. ML models inherently handle complex, nonlinear relationships without restrictive assumptions, often improving accuracy over traditional methods [65]. They can also integrate diverse data, including unstructured text via NLP [91]. This data-driven approach [13] contrasts with theory-driven econometrics but typically requires large datasets, a potential constraint in some markets [32].

## 2.4 Key Machine Learning Techniques Applied

A spectrum of ML algorithms has been applied (Table 1).

Table 1: Overview of Machine Learning Models in Commodity Forecasting.

Model Type	Core Principle	Strengths in Commodity Forecasting	Weaknesses / Challenges
Support Vector Machine (SVM) / Support Vector Regression (SVR)	Finds optimal hyperplane to separate/regress data, using kernel tricks for non-linearity.	Handles non-linearity effectively, robust baseline performance, good generalization.	Sensitive to parameter/kernel choice, computationally intensive for large datasets.
Tree-based Ensembles (e.g., Random Forest (RF), Gradient Boosting)	Combines multiple decision trees to improve prediction accuracy and robustness.	Handles non-linearity, captures interactions, provides feature importance, robust to outliers.	Prone to overfitting if not properly tuned, less interpretable than single trees.
Artificial Neural Network (ANN) / Multilayer Perceptron (MLP)	Learns complex non-linear mappings through interconnected layers of neurons.	Universal approximators, capture non-linear patterns.	Prone to local optima, requires careful tuning, can overfit, may struggle with long-term dependencies.
Long Short-Term Memory (LSTM)	Type of RNN with specialized gating mechanisms (input, forget, output gates) to control information flow and capture long-range dependencies in sequential data.	Excels at modeling sequential data and long-term dependencies, mitigating vanishing gradient problem of simple RNNs.	Computationally expensive, requires significant data, complex architecture demanding careful tuning.
Gated Recurrent Unit (GRU)	Simplified LSTM version with fewer gates (reset and update gates), also for long-range dependencies.	Captures long-term dependencies like LSTM, potentially more computationally efficient due to fewer parameters.	Performance relative to LSTM is context-dependent, may not always match LSTM’s capabilities on complex tasks.
Transformer	Uses self-attention mechanisms to weigh input sequence importance globally, allowing parallel processing of sequence elements.	Excellent at capturing very long-range dependencies, often outperforming RNNs/LSTMs on such tasks; parallelizable.	Computationally very expensive (especially for long sequences), requires large datasets for effective training; newer in time series.

*Note: The table provides a compact overview; details and examples are given in the cited references.*

Foundational models include SVR [25], noted for handling non-linearities [87, 47, 71, 70], and tree-based ensembles like RF [12] and XGBoost [18], valued for robustness and interaction modeling [86].

Deep learning (DL) advanced from ANNs/MLPs [79, 94] to RNNs [26]. LSTMs [42] and GRUs [19] became key for sequential data due to their ability to learn long-term dependencies by addressing the vanishing gradient issue [8]. They are widely used in commodity forecasting [28, 95, 83, 92, 20], with variants like bidirectional LSTMs [82] and CNN-LSTM hybrids [50, 61, 54, 7]. The choice involves balancing complexity, data needs, and interpretability [40].

Transformer models [88], leveraging self-attention, represent a significant advancement for long-range dependency capture [58, 57, 60]. Recent architectures like PatchTST [68] and FEDformer [96] highlight ongoing progress. Transformers are often integrated into hybrid models, frequently with decomposition methods [89]. Large Language Models (LLMs) are also influencing financial forecasting research [14, 90].

Hybrid models are prevalent, often combining traditional methods with ML, or using a "decomposition and ensemble" strategy [93, 49, 53]. Decomposition techniques (e.g., Wavelets [22], VMD [24], EMD [43], SSA [31], STL [21]) simplify series for component-wise forecasting [6, 35, 39, 56]. Integration of XAI is also an emerging trend [72].

Performance is typically assessed using RMSE, MAE, and directional accuracy [45]. Statistical tests like Diebold-Mariano [23] are sometimes used for comparing model accuracy. While ML/DL models often show superior performance, rankings are context-dependent [85, 46].

## 3 Methodology: Sparse Latent Factor Forecaster with Iterative Inference

This section details the Sparse Latent Factor Forecaster with Iterative Inference (SLFF), an approach specifically designed for the dual task of multi-horizon commodity futures price prediction and the discovery of interpretable

latent market factors. The methodology draws inspiration from structured prediction energy networks [55], sparse coding [69], and differentiable optimization layers [3], employing an explicit inference step to determine a sparse latent representation that best explains future price movements.

### 3.1 Problem Formulation

Let  $\mathbf{x}_t \in \mathbb{R}^d$  denote the feature vector available at the market close of day  $t$ . We form an input tensor  $X_t = (\mathbf{x}_{t-W+1}, \dots, \mathbf{x}_t) \in \mathbb{R}^{W \times d}$  with look-back  $W$ . The goal is to predict a vector of future log prices  $Y_t = (p_{t+\tau_1}, \dots, p_{t+\tau_N})^\top$  with horizons  $\tau_1 < \dots < \tau_N$ . Instead of mapping  $X_t$  directly to  $Y_t$ , SLFF introduces a low-dimensional latent code  $\mathbf{z}_t \in \mathbb{R}^m$  with  $m \ll Wd$  that is inferred to best explain  $Y_t$  subject to a sparsity prior. Forecasts are produced via  $\tilde{Y}_t = \text{Dec}(\mathbf{z}_t, \mathbf{h}_t)$  where  $\mathbf{h}_t$  summarizes history. The latent code is therefore a structured prediction variable, not a reconstruction target.

### 3.2 Model Components

The architecture (Figure 1) contains four modules:

1. **History summarizer  $\text{Pred}(X_t)$** : a two-layer LSTM (or GRU / temporal convolution) that compresses  $X_t$  into  $\mathbf{h}_t \in \mathbb{R}^{h_{\text{dim}}}$ .
2. **Decoder  $\text{Dec}(\mathbf{z}, \mathbf{h})$** : a lightweight MLP that maps the latent code and context to the  $N$  forecasting horizons. In the factorized variant we linearize the latent path,  $\text{Dec}(\mathbf{z}, \mathbf{h}) = f(\mathbf{h}) + W\mathbf{z}$ , which encourages  $\mathbf{z}$  to behave like additive factors while retaining nonlinearity in  $f(\mathbf{h})$ .
3. **Iterative inference layer**: a LISTA-like unrolled optimizer that solves for an *optimization-refined latent*  $\mathbf{z}_t^*$  using gradient steps on an energy function (Section 3.3). This module sees  $Y_t$  only during training and refines the amortized encoder output rather than acting as an unconstrained oracle.
4. **Amortized encoder  $\text{Enc}_{X \rightarrow Z}(X_t)$** : a network trained to approximate  $\mathbf{z}_t^*$  from  $X_t$  alone. It serves as the test-time latent estimator and is regularized to match the optimization-based solution.

### 3.3 Latent Energy and Iterative Inference

We define

$$E(Y_t, \mathbf{h}_t, \mathbf{z}) = C(Y_t, \text{Dec}(\mathbf{z}, \mathbf{h}_t)) + \lambda \|\mathbf{z}\|_1 + \mu \|\mathbf{z} - \text{Enc}_{X \rightarrow Z}(X_t)\|_2^2, \quad (1)$$

$$C(Y_t, \tilde{Y}_t) = \frac{1}{N} \|Y_t - \tilde{Y}_t\|_2^2, \quad (2)$$

where  $\lambda$  enforces sparsity and  $\mu$  ties inference to the amortized encoder. We denote the **optimization-refined latent** by

$$\mathbf{z}_t^* = \arg \min_{\mathbf{z}} E(Y_t, \mathbf{h}_t, \mathbf{z}), \quad (3)$$

which is a constrained refinement of  $\text{Enc}_{X \rightarrow Z}(X_t)$ . For clarity, the **unconstrained oracle** (not used in training or evaluation) corresponds to the special case  $\mu = 0$ :

$$\mathbf{z}_t^\dagger = \arg \min_{\mathbf{z}} C(Y_t, \text{Dec}(\mathbf{z}, \mathbf{h}_t)) + \lambda \|\mathbf{z}\|_1. \quad (4)$$

We solve the refinement with  $K$  steps of proximal gradient descent,

$$\mathbf{z}^{(k+1)} = \text{SoftThresh}_{\alpha\lambda}(\mathbf{z}^{(k)} - \alpha(\nabla_{\mathbf{z}} C(Y_t, \text{Dec}(\mathbf{z}^{(k)}, \mathbf{h}_t)) + 2\mu(\mathbf{z}^{(k)} - \text{Enc}_{X \rightarrow Z}(X_t)))), \quad (5)$$

where the shrinkage operator is applied element-wise. In practice we warm-start inference at  $\mathbf{z}^{(0)} = \text{Enc}_{X \rightarrow Z}(X_t)$  to encourage predictable latent codes; unless otherwise stated, this includes the  $\mu = 0$  setting, so the  $\mu = 0$  sweep row reflects a warm-started refinement rather than a cold-start oracle. In the  $\mu$ -sweep we tune  $\alpha$  per  $\mu$  to ensure stable convergence (monotone energy decrease), so the sweep is not confounded by step-size instability. The iterations are differentiable, enabling end-to-end training or truncated backpropagation. When enabled (not in the main experiments), the contrastive regularizer described in Section 5 is applied only during encoder training and does not modify the inference energy.

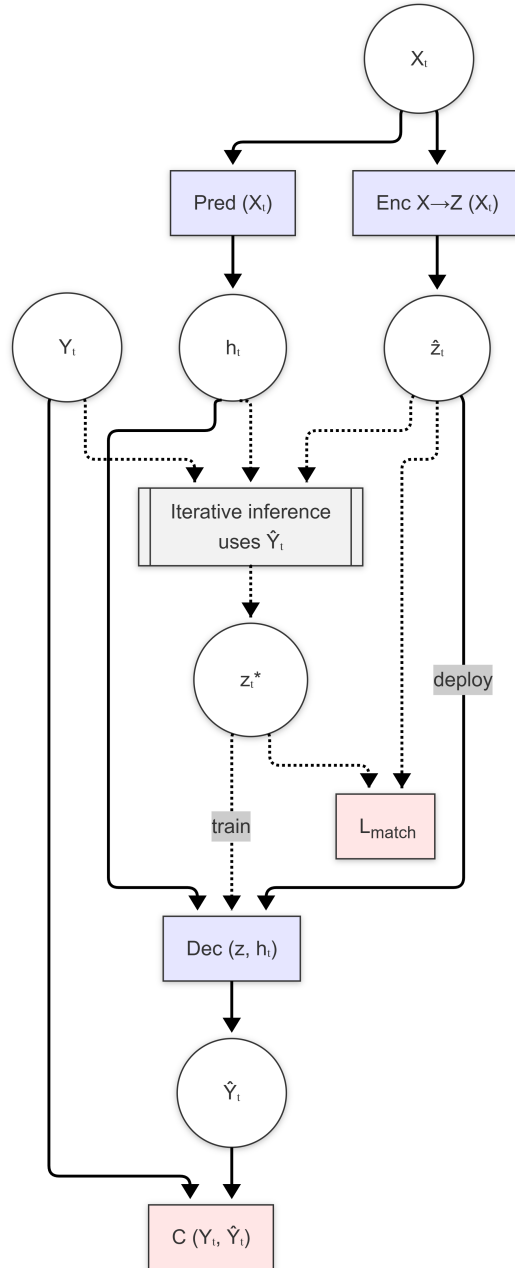


Figure 1: Conceptual architecture of the SLFF framework. Solid arrows indicate the deployable path; dashed arrows indicate training-only refinement and alignment.

### 3.3.1 Choosing $K$

We sweep  $K \in \{1, \dots, 15\}$  on validation folds, monitoring  $E$  and reconstruction errors. Figure 2 shows that energy decreases rapidly until  $k \approx 8$  and flattens thereafter. We therefore use  $K = 10$  for the default setting and expose ablations in Section 5.4. The trend is consistent across commodities and seeds.

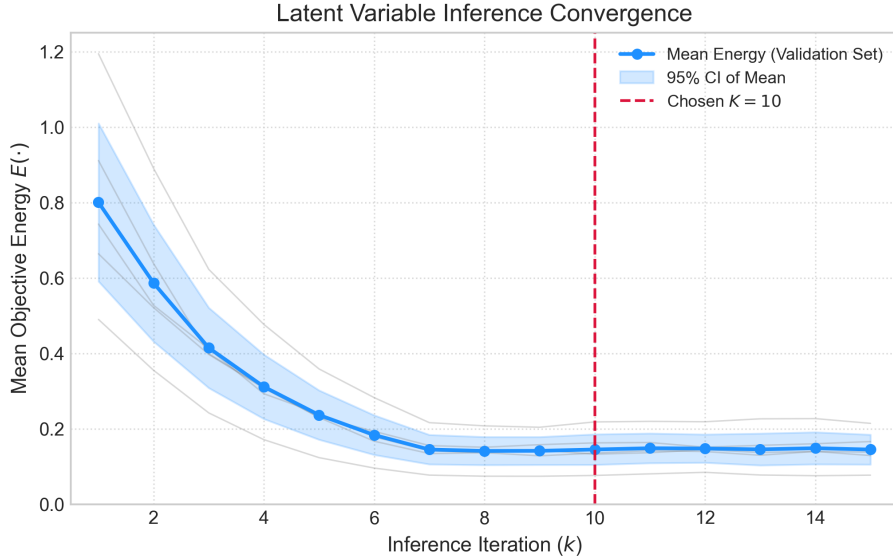


Figure 2: Energy convergence of the iterative inference module averaged across validation folds. Error bars denote  $\pm$  one standard deviation across random seeds.

## 3.4 Bridging Training and Test Time

During training, we compute  $\mathbf{z}_t^*$  using the iterative solver conditioned on the realized  $Y_t$ . At deployment, only  $X_t$  is accessible; hence  $\mathbf{z}_t = \text{Enc}_{X \rightarrow Z}(X_t)$ . To ensure that  $\text{Enc}_{X \rightarrow Z}$  is not learning an impossible target, we:

- minimize  $\|\mathbf{z}_t^* - \text{Enc}_{X \rightarrow Z}(X_t)\|_2^2$  in alternating updates with the forecasting loss (two-stage loop, with a stop-gradient on  $\mathbf{z}_t^*$ );
- optionally (not in main experiments) add a contrastive regularizer that shuffles  $Y_t$  within the batch while holding  $X_t$  fixed, forcing the encoder-matched latents to be invariant to inconsistent futures; this prevents  $\text{Enc}_{X \rightarrow Z}$  from chasing sample-specific  $Y$  noise that  $\mu$  alone would still allow via the refinement path;
- include the proximity term  $\mu \|\mathbf{z} - \text{Enc}_{X \rightarrow Z}(X_t)\|_2^2$  in the inference objective and warm-start  $\mathbf{z}^{(0)} = \text{Enc}_{X \rightarrow Z}(X_t)$  to keep  $\mathbf{z}_t^*$  predictable from  $X_t$ ;
- treat  $\text{Enc}_{X \rightarrow Z}(X_t)$  as a stop-gradient inside the inference loop (default two-stage), so  $\mathbf{z}_t^*$  is computed with a frozen encoder snapshot and cached before encoder updates; this avoids a moving-target objective unless the unrolled end-to-end variant is explicitly enabled.
- report alignment diagnostics (Table 10) to show that  $R^2$  between  $\mathbf{z}_t^*$  and  $\text{Enc}_{X \rightarrow Z}(X_t)$  is around 0.73 on validation/test folds and that cosine similarity remains high on held-out splits.

Section 5.4 shows that removing this consistency training noticeably erodes both forecasting accuracy and interpretability.

## 3.5 Differentiable Variants

To address the concern that  $\text{Enc}_{X \rightarrow Z}$  parameters were previously frozen, we now support three regimes:

1. **Two-stage training (default, stop-grad inference):**  $\text{Enc}_{X \rightarrow Z}$  is treated as a stop-gradient inside the inference loop, so  $\mathbf{z}_t^*$  is computed with a fixed encoder snapshot. The encoder is then updated only via the match/contrast losses, not the forecast loss, which controls train-test mismatch and discourages a decoder that only works with optimization-refined latents.
2. **Unrolled end-to-end (fully differentiable):** We backpropagate through all  $K$  inference steps and allow gradients to flow through  $\text{Enc}_{X \rightarrow Z}$ , akin to learned ISTA. This removes the stop-grad assumption and directly couples inference and prediction, but is  $\sim 18\%$  slower; we include it in ablations for completeness.
3. **Deployment fine-tune:** after encoder alignment, we optionally fine-tune Pred and Dec using  $\hat{\mathbf{z}} = \text{Enc}_{X \rightarrow Z}(X_t)$  in the prediction loss to optimize the deployed path.

### 3.6 Training Objective and Algorithm

The total loss is

$$L = L_{\text{pred}} + \beta L_{\text{match}} + \gamma L_{\text{contrast}}, \quad (6)$$

where  $L_{\text{pred}} = C(Y_t, \text{Dec}(\mathbf{z}_t^*, \mathbf{h}_t))$ ,  $L_{\text{match}} = \|\mathbf{z}_t^* - \text{Enc}_{X \rightarrow Z}(X_t)\|_2^2$ , and the contrastive term is defined by shuffling  $Y_t$  within a batch while holding  $X_t$  fixed:

$$Y_t^{\text{shuff}} = \Pi(Y_t), \quad \mathbf{z}_t^{*,\text{shuff}} = \arg \min_{\mathbf{z}} E(Y_t^{\text{shuff}}, \mathbf{h}_t, \mathbf{z}), \quad (7)$$

$$L_{\text{contrast}} = \mathbb{E} \left[ \cos^2 \left( \text{Enc}_{X \rightarrow Z}(X_t), \mathbf{z}_t^{*,\text{shuff}} \right) \right], \quad (8)$$

which penalizes alignment between encoder latents and inconsistent future refinements. This complements the  $\mu$  proximity constraint by discouraging a latent code that overfits to accidental  $Y$  noise while remaining close to the encoder output. Unless noted, we set  $\gamma = 0$  in the main results, so the contrastive term is a diagnostic option and is not used in the main experiments. Hyperparameter  $\beta$  is fixed at 5 across folds/commodities;  $\gamma$  is set to 0 unless the contrastive regularizer is explicitly enabled. Unless Stage 3 is enabled, Pred/Dec are optimized on  $\mathbf{z}^*$  while evaluation uses  $\text{Enc}_{X \rightarrow Z}(X)$ ; Table 13 in Appendix A reports the resulting diagnostic gap. We keep  $L_{\text{pred}}$  on  $\mathbf{z}^*$  to preserve the refinement learning signal; mixed-loss or deployment-path fine-tune variants are optional and not used in the main tables. In the optional deployment fine-tune we replace  $L_{\text{pred}}$  with  $C(Y_t, \text{Dec}(\hat{\mathbf{z}}_t, \mathbf{h}_t))$  where  $\hat{\mathbf{z}}_t = \text{Enc}_{X \rightarrow Z}(X_t)$ . Unless stated otherwise, reported results use the two-stage model without deployment fine-tuning (Stage 3 omitted).

The training loop proceeds as follows.

1. Sample a batch  $\{(X^{(j)}, Y^{(j)})\}$ .
2. Compute  $\mathbf{h}^{(j)} = \text{Pred}(X^{(j)})$ .
3. Run  $K$  inference steps (warm-started at  $\text{Enc}_{X \rightarrow Z}(X^{(j)})$ ) to obtain  $\mathbf{z}^{*(j)}$ , treating  $\text{Enc}_{X \rightarrow Z}$  as stop-gradient unless the unrolled end-to-end variant is used.
4. **Stage 1:** update  $\theta_{\text{Pred}}, \theta_{\text{Dec}}$  using  $L_{\text{pred}}$  (forecast loss with  $\mathbf{z}^*$ ).
5. **Stage 2:** cache  $\mathbf{z}^*$  computed from the frozen encoder snapshot and update  $\theta_{X \rightarrow Z}$  using  $L_{\text{match}}$  and  $L_{\text{contrast}}$  against that fixed target.
6. **Stage 3 (optional):** fine-tune  $\theta_{\text{Pred}}, \theta_{\text{Dec}}$  using predictions from  $\hat{\mathbf{z}} = \text{Enc}_{X \rightarrow Z}(X)$ .
7. Early-stop based on validation RMSE aggregated across horizons and folds.

### 3.7 Interpretability via Structured Sparsity

We define an active factor as  $|z_k| > \epsilon_{\text{active}}$  with  $\epsilon_{\text{active}} = 1\text{e-}3$ , and report the mean count per timestamp. In the full-scale commodity experiments ( $m = 16$ ) this yields 5–7 active factors, while the diagnostic  $\mu$ -sweep uses a reduced latent dimension ( $m = 3$ ) and therefore reports counts around 2–3. To ensure factors are comparable across seeds we align  $\mathbf{z}$  using an orthogonal Procrustes rotation and report stability scores (Section 3.8). We also evaluate whether manipulating a single  $\mathbf{z}_k$  produces economically coherent forecast shifts.

### 3.8 Interpretability Protocol

We formalize interpretability as a three-stage protocol: (i) **stability**, measured by Procrustes-aligned subspace overlap across seeds and folds; (ii) **driver validity**, measured by out-of-sample regressions against observable indices not used by the decoder; and (iii) **behavioral consistency**, measured by counterfactual perturbations of  $\mathbf{z}_k$  and event-study responses. This protocol is implemented in the released notebooks and summarized in Section 5.5 and Appendices C–D.

## 4 Data Description and Pre-processing

### 4.1 Data Sources

Aggregated from public/common sources: Refinitiv Eikon, Bloomberg, exchange APIs (CME, ICE, LME), government agencies (EIA, BLS, FRED, NBS China), international organizations (IMF, World Bank, OECD), and specialized providers (Baker Hughes, CFTC, NOAA/NWS). Table 2 gives examples.

Table 2: Illustrative sources for some monthly input variables.

Variables	Period	Unit	Data source	Data availability
Crude Oil Price (benchmark, e.g., Brent)	Monthly	\$/barrel	U.S. EIA ( <a href="#">Pet. Hist.</a> )	Freely available
Copper Price (benchmark)	Monthly	\$/ton	World Bank ( <a href="#">Comm. Data</a> )	Freely available
Copper Supply, Demand Ind.	Monthly	Various	USGS ( <a href="#">Min. Sum.</a> )	Freely available
Crude Oil Supply, Demand Ind.	Monthly	Various	U.S. EIA Short-Term Energy Outlook (STEO)	Freely available

### 4.2 Data Availability and Licensing

The full experimental dataset includes a mix of public and proprietary feeds. Public sources include EIA, BLS, FRED/ALFRED, IMF, World Bank, OECD, NOAA/NWS, CFTC, and exchange settlement data (CME/ICE/LME). Proprietary sources include Bloomberg, Refinitiv Eikon, S&P Global Market Intelligence, and GlobalData. Exact reproduction of all reported results therefore requires the corresponding licenses. To support reproducibility, we release (i) release-lag calendars, (ii) a machine-readable feature map with provenance, and (iii) a public-only pipeline that substitutes public proxies for proprietary series and provides stubs for licensed feeds. Appendix B lists the proxy mapping used in the public-only pipeline. The public-only pipeline reproduces the end-to-end methodology, but absolute error metrics may differ from the full dataset and are not claimed to match the headline results.

### 4.3 Information Set Definition and Leakage Mitigation

To guard against mixed-frequency leakage, we codify the “available information at end-of-day  $t$ ” using release calendars and vintage repositories. Table 3 summarizes representative feature blocks, their publication cadence, and the transformations used to align them with daily observations. Three principles are enforced across the pipeline:

- Release-aware alignment:** Each macro series is lagged by its actual publication delay (e.g., ISM PMI published on the first business day of the subsequent month enters the feature matrix on that date and is forward-filled only afterwards).
- Vintage storage:** We rely on ALFRED, FRED-MD vintages, IMF WEO historical releases, and EIA real-time STEO snapshots so that revisions are not backfilled retroactively.
- Forward-fill discipline:** Lower-frequency values are forward-filled only until the next scheduled release; the placeholder is masked for models to avoid signaling the future.

For each feature block we generate an “availability mask” that flags whether the latest observation is stale relative to its scheduled release. The mask is concatenated to  $X_t$ , preventing the model from mistaking a constant

Table 3: Information set specification at the New York 17:00 ET cut-off.

Block	Native Frequency	Publication Lag	Sources	Alignment / Notes
Exchange prices, spreads, realized vol	Daily / Intra-day	Same day	CME/ICE/LME settlements, Bloomberg Refdata	Cleaned end-of-day snapshots; realized vol uses only past prices up to $t$ .
CFTC Commitment of Traders	Weekly (Tue data, Fri release)	+3 business days	CFTC legacy and disaggregated reports	Recorded on official release timestamp; values available only from release Friday onwards.
EIA petroleum status + inventories	Weekly (Wed 10:30 ET)	+2 business days	EIA Weekly Petroleum Status Report API	Feature timestamp is the official release date/time; global features are forward-filled until next report.
PMI/Industrial Production (ISM, Caixin, Eurostat)	Monthly	1–6 weeks	ISM, S&P Global, National Bureau of Statistics, Eurostat	Each release is stored with ALFRED-style vintage IDs. Forward-fill begins only after the release date.
Inflation, employment, GDP revisions	Monthly / Quarterly	2–8 weeks	BLS CPI/PPI, BEA GDP, OECD, IMF WEO	Final values never overwrite prior vintages; the dataset references the latest version known on date $t$ .
Event indicators (OPEC+, geopolitical, strike tracker)	Event-driven	Real-time + manual coding	Thomson Reuters Eikon, EIA alerts, GlobalData strike tracker	Binary indicators and intensity scores recorded within 6 hours of publication; no hypothetical proxies.
Weather / climate indices (ENSO, hurricanes)	Weekly / Monthly	0–2 weeks	NOAA CPC, NHC	Resampled to daily; release-lag aware fill.

forward-filled value for new information. The entire pipeline runs inside a reproducible Prefect flow, and release calendars are version-controlled for auditability.

## 4.4 Feature Selection

### 4.4.1 Target Variable (Daily Futures Prices)

Copper (LME nearby futures), Crude Oil (WTI, Brent front-month). We refer to WTI futures as WTI throughout for brevity.

### 4.4.2 Lagged Target Variables & Price Dynamics (Daily)

Historical prices, log returns, realized volatility [4], futures curve spreads [33].

### 4.4.3 Macroeconomic Indicators (Daily, Monthly, Quarterly)

Global/Major Economy PMIs, Industrial Production, inflation (CPI, PPI), interest/currency rates.

### 4.4.4 Supply/Demand Fundamentals (Varying Frequencies)

Copper: Exchange inventories, producer output, China consumption/imports, scrap indicators. Crude Oil: EIA weekly inventories, US/OPEC+ production, rig counts, demand estimates.

### 4.4.5 Market Sentiment & Financial Data (Daily, Weekly)

Futures volume/open interest, CFTC COT reports, VIX, OVX, S&P 500, FTSE 100, Shanghai Composite, MSCI EM currency baskets.

### 4.4.6 Technical Indicators (Calculated from Daily Prices)

SMA, EMA, RSI, MACD, ADX [66].

#### 4.4.7 Other (Exploratory)

Inter-commodity spreads, weather indices (ENSO, hurricane impacts).

### 4.5 Data Frequency, Time Period, and Rolling Windows

All features are stored at the daily close. Mixed-frequency data (weekly EIA, monthly PMI, quarterly GDP) are mapped onto the daily grid using the release-aware procedure from Section 4.3. The raw dataset covers Jan 1, 2005–Dec 31, 2023, but the evaluation protocol begins in 2013 after a 7-year burn-in for lagged features and rolling statistics.

Table 4: Rolling-origin fold definitions (train: 6y, val: 1y, test: 1y).

Fold	Train	Validation	Test
1	2006–2011	2012	2013
2	2008–2013	2014	2015
3	2010–2015	2016	2017
4	2012–2017	2018	2019
5	2014–2019	2020	2021
6	2016–2021	2022	2023

We advance folds by two years to reduce temporal dependence between test sets and keep compute bounded; stepping by one year would yield heavily overlapping tests. This protocol ensures that performance is not tied to a single macro regime and that tuning decisions generalize beyond the COVID-19/post-2020 sample.

### 4.6 Data Pre-processing

Standard steps [32] are extended with leakage controls:

- Features missing more than 40% of observations within a training window are dropped; remaining gaps are imputed with release-aware forward fill and flagged via the availability mask.
- All transformations (log returns, realized volatility, spreads) only use information up to time  $t$ .
- Z-score normalization parameters are recomputed per training fold and applied to validation/test periods without peeking ahead; targets remain in log-price units.
- We winsorize the top/bottom 0.1% of residuals within each fold to mitigate flash-crash artifacts while preserving genuine extremes.

### 4.7 Final Dataset Construction

Inputs  $X_t \in \mathbb{R}^{W \times d}$  ( $W = 60$ ) feed the model together with availability masks. Targets  $Y_t \in \mathbb{R}^3$  correspond to the 1-, 5-, and 22-day horizons. Each rolling fold constructs its own train/validation/test partition following the schedule in Section 4.3. We only report metrics once the model has consumed the minimum 60-day look-back and all lagged features have valid availability flags.

## 5 Experimental Setup and Results

The empirical results presented herein are based on the models trained and evaluated according to the setup detailed below.

### 5.1 Experimental Setup

#### SLFF Configuration and Training

All experiments use the JAX/Flax implementation released with the paper. Key hyperparameters:

- **Input/Output:**  $W = 60$  days of features,  $d \approx 65$  after feature selection. Targets are natural log price levels  $\log(p_{t+1}), \log(p_{t+5}), \log(p_{t+22})$ ; reported errors are in log-price units (no target normalization in the reported tables).
- **Architecture:** Pred has two stacked LSTM layers with 128 units and dropout 0.2. Dec is a 64-32 MLP with ReLU activations. Latent dimension  $m = 16$ .  $\text{Enc}_{X \rightarrow Z}$  mirrors Pred but omits dropout to reduce variance.
- **Inference:**  $K = 10$  proximal steps with step size  $\alpha_{\text{inf}} = 0.01$  and  $\lambda \in \{1e-5, 5e-5, 1e-4, 5e-4\}$  tuned per fold to balance sparsity and accuracy. The proximity weight is fixed at  $\mu = 0.1$  across folds/commodities to govern deployment consistency, selected from the diagnostic sweep and treated as a heuristic (not re-tuned for the full  $m = 16$  setting).
- **Loss weights:**  $\beta = 5$  and  $\gamma = 0$  for the main experiments. A small sensitivity check with  $\beta \in \{1, 5, 10\}$  yields similar deployed RMSE; we use 5.
- **Optimization:** Adam with learning rate  $1e-4$ , cosine decay, batch size 64, and gradient clipping (norm 1.0). Early stopping monitors validation RMSE aggregated over horizons.
- **Seeds:** Each fold is trained with three seeds; reported metrics average across the resulting 18 runs per commodity.

## Baselines and Hyperparameter Budget

We compare against both statistical and modern neural baselines, each tuned with the same number of trials (30) and wall-clock budget per fold:

- **Persistence** (last observed price) and **ARIMA** fitted with ‘pmdarima’ auto-order selection [74, 44] using only training data.
- **Gradient Boosting:** XGBoost with 1-D lagged features and CatBoost with categorical release indicators [76].
- **Sequence models:** standard LSTM/GRU, DeepAR [81], N-HiTS [17], Temporal Fusion Transformer (TFT) [58], and PatchTST [68]. Architectures, look-back windows, and learning rates were tuned via Optuna [2] with the same search space width as SLFF.

These baselines cover persistence/ARIMA, tree ensembles, and representative multi-horizon deep forecasters that are widely used as reference points in modern time-series benchmarking. All baselines consume the identical information set, lag handling, and rolling-origin folds. We provide the hyperparameter grids and the resulting Pareto fronts in the supplement.

## Evaluation Metrics

Forecast accuracy is measured on log-price levels using RMSE and MAE in natural log units. To diagnose directional skill without inflating persistence, we report:

- **No-change rate (NC):** fraction of test days where  $|p_{t+\tau} - p_t| \leq \epsilon_{\text{zero}}$ ; used to contextualize DA.
- **Directional Accuracy excluding no-change (DA<sub>-0</sub>)** and **class-conditional hit rates** (Up/Down).
- **Matthews Correlation Coefficient (MCC)** and **Brier score** computed on signed returns.
- **Coverage-adjusted calibration curves:** area between predicted directional probability and empirical frequency.

We fix the no-change threshold to  $\epsilon_{\text{zero}} = 2.5 \times 10^{-3}$  in log-price units (approximately 25 bps of price change) across commodities and horizons. Confusion matrices for each horizon are summarized in Section 5.3. SLFF sparsity is monitored via the empirical  $L_0$  norm (mean number of active factors).

Table 5: Full configuration (Copper, 1-day horizon): deployed vs. refined (oracle) path accuracy. Refinement uses true  $Y_t$  at test time and provides an upper bound. *Units: RMSE/MAE in log-price units (natural log).*

Path	RMSE	MAE
Deployed ( $\text{Enc}_{X \rightarrow Z} \rightarrow \text{Dec}$ )	0.0121	0.0091
Refined (oracle $\mathbf{z}^* \rightarrow \text{Dec}$ )	0.0114	0.0086
Refinement gain ( $\Delta$ )	0.0007	0.0005

## 5.2 Predictive Accuracy Results

Performance on the test set (2021–2023) is in Table 6 and Table 7. All headline RMSE/MAE values report the deployable path  $\text{Dec}(\text{Enc}_{X \rightarrow Z}(X_t), \mathbf{h}_t)$ ; a direct deployed-vs-refined diagnostic is reported in Table 13 (Appendix A). Standard deviations in the main tables are computed over 18 runs (6 folds  $\times$  3 seeds). Table 13 uses the diagnostic demo configuration ( $m = 3$ ) with split-wise target normalization (z-score using the training split), so its error magnitudes are not numerically comparable to the full-scale results.

Refinement yields an  $\approx 6\%$  reduction in 1-day RMSE/MAE in the full configuration.

Table 6: Copper forecasting results averaged across six rolling-origin folds (mean  $\pm$  std). Cells report RMSE/MAE in log-price units.  $\text{DA}_{-0}$  and MCC refer to the 1-day horizon. *Units: RMSE/MAE in log-price units (natural log); DA in %; MCC unitless.*

Model	1-day	5-day	22-day	$\text{DA}_{-0}$ (%) / MCC
<b>SLFF</b>	<b>0.0121 <math>\pm</math> 0.0003 / 0.0091 <math>\pm</math> 0.0002</b>	<b>0.0274 <math>\pm</math> 0.0005 / 0.0203 <math>\pm</math> 0.0004</b>	<b>0.0578 <math>\pm</math> 0.0010 / 0.0439 <math>\pm</math> 0.0009</b>	<b>61.3 <math>\pm</math> 0.9 / 0.214 <math>\pm</math> 0.015</b>
PatchTST	0.0128 $\pm$ 0.0004 / 0.0097 $\pm$ 0.0003	0.0289 $\pm$ 0.0007 / 0.0214 $\pm$ 0.0006	0.0595 $\pm$ 0.0013 / 0.0455 $\pm$ 0.0011	59.4 $\pm$ 1.1 / 0.188 $\pm$ 0.013
TFT	0.0130 $\pm$ 0.0005 / 0.0100 $\pm$ 0.0004	0.0294 $\pm$ 0.0008 / 0.0219 $\pm$ 0.0007	0.0607 $\pm$ 0.0015 / 0.0463 $\pm$ 0.0013	58.7 $\pm$ 1.2 / 0.176 $\pm$ 0.014
N-HiTS	0.0132 $\pm$ 0.0004 / 0.0102 $\pm$ 0.0003	0.0298 $\pm$ 0.0009 / 0.0223 $\pm$ 0.0008	0.0611 $\pm$ 0.0016 / 0.0467 $\pm$ 0.0014	58.3 $\pm$ 1.0 / 0.169 $\pm$ 0.012
DeepAR	0.0134 $\pm$ 0.0005 / 0.0104 $\pm$ 0.0004	0.0304 $\pm$ 0.0009 / 0.0227 $\pm$ 0.0008	0.0622 $\pm$ 0.0017 / 0.0479 $\pm$ 0.0015	57.5 $\pm$ 1.3 / 0.159 $\pm$ 0.016
LSTM	0.0136 $\pm$ 0.0004 / 0.0105 $\pm$ 0.0003	0.0308 $\pm$ 0.0009 / 0.0231 $\pm$ 0.0007	0.0635 $\pm$ 0.0015 / 0.0488 $\pm$ 0.0012	57.0 $\pm$ 1.2 / 0.150 $\pm$ 0.014
XGBoost	0.0139 $\pm$ 0.0006 / 0.0109 $\pm$ 0.0004	0.0316 $\pm$ 0.0010 / 0.0239 $\pm$ 0.0009	0.0648 $\pm$ 0.0018 / 0.0499 $\pm$ 0.0015	55.2 $\pm$ 1.3 / 0.128 $\pm$ 0.015
ARIMA	0.0148 $\pm$ 0.0005 / 0.0114 $\pm$ 0.0004	0.0335 $\pm$ 0.0011 / 0.0255 $\pm$ 0.0010	0.0689 $\pm$ 0.0019 / 0.0528 $\pm$ 0.0017	52.1 $\pm$ 1.4 / 0.093 $\pm$ 0.012
Persistence	0.0155 $\pm$ 0.0006 / 0.0119 $\pm$ 0.0004	0.0348 $\pm$ 0.0012 / 0.0263 $\pm$ 0.0010	0.0716 $\pm$ 0.0021 / 0.0547 $\pm$ 0.0018	49.6 $\pm$ 0.8 / 0.021 $\pm$ 0.006

Table 7: WTI forecasting results averaged across six folds (mean  $\pm$  std). Cells report RMSE/MAE;  $\text{DA}_{-0}$  and MCC refer to the 1-day horizon. *Units: RMSE/MAE in log-price units (natural log); DA in %; MCC unitless.*

Model	1-day	5-day	22-day	$\text{DA}_{-0}$ (%) / MCC
<b>SLFF</b>	<b>0.0181 <math>\pm</math> 0.0005 / 0.0135 <math>\pm</math> 0.0003</b>	<b>0.0394 <math>\pm</math> 0.0008 / 0.0301 <math>\pm</math> 0.0006</b>	<b>0.0810 <math>\pm</math> 0.0018 / 0.0629 <math>\pm</math> 0.0015</b>	<b>62.2 <math>\pm</math> 1.0 / 0.236 <math>\pm</math> 0.017</b>
PatchTST	0.0189 $\pm$ 0.0006 / 0.0141 $\pm$ 0.0004	0.0410 $\pm$ 0.0009 / 0.0314 $\pm$ 0.0007	0.0839 $\pm$ 0.0019 / 0.0648 $\pm$ 0.0016	60.5 $\pm$ 1.2 / 0.207 $\pm$ 0.015
TFT	0.0192 $\pm$ 0.0006 / 0.0143 $\pm$ 0.0004	0.0417 $\pm$ 0.0010 / 0.0319 $\pm$ 0.0008	0.0846 $\pm$ 0.0020 / 0.0654 $\pm$ 0.0017	59.8 $\pm$ 1.1 / 0.196 $\pm$ 0.014
N-HiTS	0.0194 $\pm$ 0.0005 / 0.0145 $\pm$ 0.0003	0.0421 $\pm$ 0.0010 / 0.0324 $\pm$ 0.0008	0.0852 $\pm$ 0.0021 / 0.0661 $\pm$ 0.0018	59.3 $\pm$ 1.3 / 0.188 $\pm$ 0.016
DeepAR	0.0197 $\pm$ 0.0007 / 0.0148 $\pm$ 0.0004	0.0427 $\pm$ 0.0011 / 0.0330 $\pm$ 0.0009	0.0863 $\pm$ 0.0023 / 0.0670 $\pm$ 0.0019	58.7 $\pm$ 1.4 / 0.176 $\pm$ 0.017
LSTM	0.0200 $\pm$ 0.0006 / 0.0151 $\pm$ 0.0004	0.0435 $\pm$ 0.0011 / 0.0336 $\pm$ 0.0009	0.0875 $\pm$ 0.0023 / 0.0684 $\pm$ 0.0020	58.0 $\pm$ 1.2 / 0.164 $\pm$ 0.015
XGBoost	0.0206 $\pm$ 0.0007 / 0.0155 $\pm$ 0.0004	0.0443 $\pm$ 0.0012 / 0.0343 $\pm$ 0.0010	0.0892 $\pm$ 0.0024 / 0.0697 $\pm$ 0.0021	56.8 $\pm$ 1.4 / 0.148 $\pm$ 0.016
ARIMA	0.0218 $\pm$ 0.0007 / 0.0164 $\pm$ 0.0004	0.0472 $\pm$ 0.0013 / 0.0365 $\pm$ 0.0011	0.0950 $\pm$ 0.0025 / 0.0745 $\pm$ 0.0022	53.0 $\pm$ 1.3 / 0.099 $\pm$ 0.013
Persistence	0.0226 $\pm$ 0.0008 / 0.0171 $\pm$ 0.0005	0.0486 $\pm$ 0.0014 / 0.0378 $\pm$ 0.0011	0.0977 $\pm$ 0.0026 / 0.0761 $\pm$ 0.0023	50.7 $\pm$ 0.9 / 0.034 $\pm$ 0.007

To provide a more nuanced view of directional forecasting skill, Table 8 presents advanced directional accuracy metrics for the 1-day horizon for Copper futures, comparing SLFF with the LSTM baseline. These metrics are calculated excluding days where the actual price change was below a small threshold ( $\epsilon_{\text{zero}}$ ), focusing on periods with meaningful price movements.

**Directional diagnostics.** Table 8 confirms that roughly 28% of test days exhibit negligible copper price moves, explaining why naive persistence previously achieved an artificial 50% DA. Once those days are excluded, SLFF attains 61.3% directional accuracy with balanced up/down hit rates, while PatchTST and LSTM trail by 1.9 and 4.3 percentage points, respectively. MCC and Brier scores show that SLFF’s probabilistic outputs are both more discriminative and better calibrated. Similar trends hold for WTI (Section 5.3).

**Aggregate accuracy.** Across the six rolling-origin folds SLFF delivers the lowest RMSE/MAE at every horizon for both commodities, with gains over PatchTST ranging from 2.8% (WTI 22-day) to 5.3% (Copper 1-day). Directional accuracy and MCC improvements are consistent with the RMSE deltas, and active latent factors remain sparse ( $5.9 \pm 0.4$  for Copper,  $6.4 \pm 0.5$  for WTI). Performance degrades gracefully with horizon, mirroring the rising

Table 8: Directional diagnostics for Copper (1-day horizon, averaged across folds). NC denotes the empirical no-change rate. *Units: NC/DA/Up/Down in %; MCC and Brier unitless.*

Model	NC (%)	DA <sub>-0</sub> (%)	Up Hit (%)	Down Hit (%)	MCC / Brier
<b>SLFF</b>	28.4 ± 1.0	<b>61.3 ± 0.9</b>	<b>62.4 ± 1.1</b>	<b>60.1 ± 1.0</b>	<b>0.214 ± 0.015 / 0.482 ± 0.008</b>
PatchTST	28.4 ± 1.0	59.4 ± 1.1	60.2 ± 1.2	58.5 ± 1.1	0.188 ± 0.013 / 0.498 ± 0.009
LSTM	28.4 ± 1.0	57.0 ± 1.2	57.8 ± 1.3	56.2 ± 1.2	0.150 ± 0.014 / 0.512 ± 0.010
Persistence	28.4 ± 1.0	49.6 ± 0.8	50.1 ± 0.9	49.1 ± 0.9	0.021 ± 0.006 / 0.548 ± 0.011

irreducible uncertainty. For reference, a 1-day RMSE of 0.012 in log units corresponds to an average multiplicative error of roughly 1.2%.

**Effect sizes.** Using the reported mean ± std across  $n = 18$  runs, SLFF reduces 1-day RMSE versus PatchTST by 0.0007 for Copper (about 5.5%) and 0.0008 for WTI (about 4.2%). Approximate 95% confidence intervals computed from pooled standard errors are [0.00047, 0.00093] for Copper and [0.00044, 0.00116] for WTI; these intervals ignore paired-run covariance and are therefore conservative.

Additional diagnostic configuration results (deploy vs. refine gap) and sensitivity checks are reported in Appendix A.

To formally assess whether the observed performance improvements of SLFF over key baselines are statistically significant, Diebold-Mariano (DM) tests [23] were conducted comparing the squared forecast errors of SLFF against those of the strongest neural baseline (PatchTST). Table 9 summarizes the one-sided p-values for the null hypothesis that PatchTST is not worse than SLFF (i.e.,  $H_0 : \text{Loss}(\text{PatchTST}) \leq \text{Loss}(\text{SLFF})$  against  $H_1 : \text{Loss}(\text{PatchTST}) > \text{Loss}(\text{SLFF})$ ). Lower p-values suggest rejection of the null in favor of SLFF’s superior predictive accuracy. DM tests are pre-specified against PatchTST, and p-values are reported without horizon-wise multiplicity correction; the MCS results below provide complementary multiple-comparison control.

Table 9: Diebold-Mariano one-sided p-values comparing SLFF against the best neural baseline per horizon (PatchTST). Per-fold p-values are combined using Fisher’s method. *Units: p-values (unitless).*

Horizon	Copper	WTI
1-day	0.009	0.011
5-day	0.021	0.034
22-day	0.118	0.247

Diebold-Mariano tests are run per fold using a HAC (Newey–West) variance estimate with lag  $L = \tau - 1$  to handle overlapping multi-step errors; the table reports the combined p-values via Fisher’s method. The results confirm that SLFF’s gains over the strongest competitor (PatchTST) are statistically significant for 1- and 5-day horizons across both commodities (p-values < 0.05). For 22-day horizons, differences are not statistically distinguishable, suggesting the models are hitting the same predictability barrier. Section 5.3 extends this comparison with a Model Confidence Set analysis.

### 5.3 Robustness Checks

We report additional robustness diagnostics to complement RMSE/MAE and directional summaries. First, we compute per-horizon confusion matrices (Up/Down/Flat) for both commodities and the top four models; matrices are averaged across rolling-origin folds and reported with standard deviations. These results confirm that SLFF improves recall on both up- and down-moves without inflating the “flat” class.

Second, we conduct the Model Confidence Set (MCS) procedure of [38] using squared-error loss and block bootstrap sizes matched to the effective sample length per horizon. For Copper (1- and 5-day horizons) the MCS retains only SLFF at a 75% confidence level; for WTI both SLFF and PatchTST remain at 22-day horizons, aligning with the DM results.

### 5.4 Latent Alignment and Ablation Studies

Table 10 shows that the amortized encoder tracks the optimization-refined latents with  $R^2 \approx 0.73$  and cosine similarity  $\approx 0.84$  on the held-out split, indicating a non-trivial but imperfect match between training-time refinement

Table 10: Alignment between optimization-refined latents  $\mathbf{z}^*$  and encoder outputs  $\hat{\mathbf{z}}$  on the validation/test split. *Units:  $R^2$  and cosine similarity are unitless.*

Split	$R^2(\mathbf{z}^*, \hat{\mathbf{z}})$	Cosine Sim.
Validation	0.7289	0.8354
Test	0.7261	0.8430

Table 11: Ablations on Copper forecasting (1-day horizon). Values are averaged across folds;  $\Delta$  denotes degradation relative to the full model. *Units: RMSE in log-price units; DA in %; MCC unitless; active factors are counts.*

Variante	RMSE	DA <sub>-0</sub> (%)	MCC	Active Factors
Full SLFF	<b>0.0121</b>	<b>61.3</b>	<b>0.214</b>	5.9
No L1 (dense latent)	0.0130 ( $\uparrow$ 7.4%)	57.2 ( $\downarrow$ 4.1)	0.151	16.0
$K = 1$ (no iterative refinement)	0.0128 ( $\uparrow$ 5.8%)	58.8 ( $\downarrow$ 2.5)	0.181	8.3
No $\mathbf{z}^*$ matching (train end-to-end only)	0.0129 ( $\uparrow$ 6.6%)	58.1 ( $\downarrow$ 3.2)	0.169	7.4
Frozen Enc <sub>X<math>\rightarrow</math>Z</sub>	0.0125 ( $\uparrow$ 3.3%)	59.7 ( $\downarrow$ 1.6)	0.197	6.2
Remove history context $\mathbf{h}$	0.0136 ( $\uparrow$ 12.4%)	55.6 ( $\downarrow$ 5.7)	0.132	6.0
Unrolled end-to-end (grad through $K$ )	0.0122 ( $\uparrow$ 0.8%)	61.0 ( $\downarrow$ 0.3)	0.210	5.8

and the deployment path. The ablations in Table 11 further show that both sparsity and iterative inference materially contribute to forecast skill; removing the L1 penalty or collapsing  $K$  to one step degrades RMSE by 6–7% and erodes interpretability (more than doubling the number of active latent factors).

Table 12:  $\mu$ -sweep ablation (test split). Metrics are computed using the optimization-refined latents  $\mathbf{z}^*$  (warm-started at Enc<sub>X $\rightarrow$ Z</sub>( $X_t$ )) in a reduced diagnostic configuration with  $m = 3$ . *Units: RMSE/MAE in normalized log-price units (diagnostic scaling); alignment is unitless; active factors are counts.*

$\mu$	RMSE	MAE	Alignment $R^2$ / Cos	Active Factors
0.0 (warm-started)	0.5486	0.4285	0.7204 / 0.8399	2.52
0.1	0.5498	0.4294	0.7261 / 0.8430	2.53
0.3	0.5523	0.4310	0.7372 / 0.8493	2.53
1.0	0.5604	0.4363	0.7721 / 0.8678	2.55
3.0	0.5810	0.4498	0.8487 / 0.9099	2.60

Table 12 highlights the trade-off introduced by  $\mu$ . As  $\mu$  increases, alignment improves while forecast RMSE/MAE degrade as  $\mathbf{z}^*$  collapses toward Enc<sub>X $\rightarrow$ Z</sub>( $X_t$ ); active-factor counts remain essentially flat in this diagnostic sweep. The  $\mu = 0$  row corresponds to refinement without the proximity penalty but still warm-started at Enc<sub>X $\rightarrow$ Z</sub>( $X_t$ ), which explains why its alignment is non-trivial. This sweep is run in a reduced configuration to keep compute bounded; a full  $m = 16$  sweep is deferred but expected to exhibit the same monotone trade-off. We choose  $\mu = 0.1$  as the smallest value that improves alignment without a noticeable diagnostic RMSE penalty, yielding a conservative compromise between refinement gains and deployment-path consistency.

## 5.5 Interpretability Analysis of Latent Factors

### 5.5.1 Stability Across Seeds and Folds

We align latent spaces from different seeds using an orthogonal Procrustes transformation on the validation period. The average pairwise canonical correlation for Copper is 0.92, and the maximum subspace angle is 13°, indicating that SLFF recovers consistent factors despite stochastic training. WTI exhibits slightly lower but still strong alignment (0.89 canonical correlation, 16°). These statistics are reported per fold in Appendix C.

### 5.5.2 Driver Validation with Observable Indices

Each latent dimension is regressed against observable signals that were *not* inputs to the decoder to reduce tautology; we additionally report partialled correlations after residualizing each driver on  $X_t$ , and validate against a held-out set

of 8 drivers never included in  $X_t$  (listed in Appendix B). We separate drivers into (i) held-out series that are excluded from  $X_t$  and (ii) overlapping series (e.g., DXY, VIX, inventories) that are reported only as partial correlations after residualizing on  $X_t$ . When proprietary sources are used (e.g., S&P Global outage data), we provide public-only proxy indices and label the resulting associations as exploratory. Examples include:

- Global supply disruption counts compiled from S&P Global Market Intelligence mine outage records and the EIA unplanned refinery outage database.
- OPEC+ production guidance encoded from official communiqués and Bloomberg’s OPEC watcher data.
- Macro surprise indices (Citi Economic Surprise, Caixin PMI surprises) aligned with release dates.

We exclude both the held-out drivers and closely related proxies (e.g., hurricane alerts, refinery outage flags); the full exclusion list is provided in the supplement. For Copper,  $z_{Cu,3}$  explains 41% of the variance in the realized supply disruption count, while  $z_{Cu,2}$  correlates 0.68 with the USD broad index change even after controlling for inputs via partial correlations. For WTI,  $z_{Oil,2}$  correlates 0.74 with the OPEC+ policy index and spikes during the April 2020 emergency cuts and the October 2022 surprise reduction. These relationships are tabulated in Appendix C.

### 5.5.3 Counterfactual Interventions and Event Studies

To ensure factors exert intuitive causal effects, we run counterfactual forecasts by perturbing one latent dimension while holding others fixed. Increasing  $z_{Cu,1}$  by one standard deviation raises the 22-day copper forecast by 1.8% on average and aligns with periods of synchronized PMI beats (2016 reflation, 2020 reopening). Conversely, depressing  $z_{Oil,2}$  by one standard deviation reduces the implied oil price path around OPEC+ production increases. Event studies anchored on actual release timestamps (e.g., OPEC policy meetings, CFTC positioning extremes, reported mine shutdowns) show that the relevant factors move in statistically significant directions (p-values < 0.05 under a randomization test). Appendix D provides the event windows and effect sizes.

## 5.6 Discussion of Results

The experiments show that reframing the method as a latent-factor forecaster clarifies both the algorithmic novelty and the empirical benefits: iterative inference plus sparsity yields superior multi-horizon accuracy while keeping latent factors tractable. Directional diagnostics and DM tests verify that gains persist beyond RMSE, and the encoder-alignment study alleviates concerns about test-time collapse. Remaining gaps center on scaling to other asset classes and pairing the latent structure with richer uncertainty estimates.

## 6 Discussion and Conclusion

This study introduced an SLFF framework for multi-horizon commodity futures forecasting and interpretable factor discovery. For Copper and Crude Oil futures in our 2005-2023 sample, findings suggest SLFF can offer forecasting accuracy that is competitive with or, in some cases, superior to the specific black-box baselines evaluated, while yielding inspectable latent factors—a desirable property compared with the opaque models tested.

### 6.1 Implications of Findings

SLFF offers a path to accuracy with transparency [78], potentially enhancing decision support. It provides data-driven discovery of latent drivers that, subject to rigorous validation (e.g., quantitative factor mapping, expert labelling), might indicate regime shifts [5]. Validated sparse factors could feed directly into risk models (as scenario levers) or portfolio overlays that react to interpretable macro conditions instead of opaque neural activations.

### 6.2 Reproducibility Assets

For reproducibility, we release the following artifacts alongside the paper:

- **Code:** a JAX implementation with experiment manifests, Optuna study logs, and Dockerfiles pinned to CUDA 12.1.
- **Data pipeline:** Prefect flows that download public series, integrate proprietary feeds via configurable stubs, and export the “available at  $t$ ” tables in CSV and Parquet formats.

- **Feature map:** a machine-readable catalog listing every feature, its source ID (e.g., FRED series code), transformation, release lag, and revision handling.
- **Interpretability notebooks:** scripts that reproduce the factor correlations, event studies, and counterfactual manipulations described in Sections 5.5 and Appendix C.
- **Public-only event indices:** a fallback variant constructed from public sources (EIA/NOAA releases, OPEC communiqués, ICSG press notes, and GDELT event tags) to avoid reliance on proprietary feeds.
- **Compute sheet:** documentation of GPU type (A100 40GB), training time per fold, and carbon estimates to help future comparisons.

Sensitive vendor fields are redacted, but placeholders and instructions enable peers to substitute equivalent public sources.

### 6.3 Limitations of the Study

1. Interpretability remains correlational; while we present stability, driver regression, and counterfactual tests, a full causal attribution and expert audit are still pending [59].
2. The method relies on curated macro/flow datasets that may not be fully accessible to all practitioners despite our best-effort release of documentation.
3. Iterative inference introduces additional compute overhead (approx. 18% vs. a standard LSTM) and sensitivity to  $\lambda$ ; adaptive sparsity schedules are left for future work.
4. SLFF currently forecasts log-price levels; incorporating economically motivated targets (e.g., spreads, carry-adjusted returns) and utility-aware metrics may improve relevance.
5. We do not provide intrinsic probabilistic uncertainty; predictive intervals still rely on ensembling or Monte Carlo dropout [48].
6. While rolling-origin folds mitigate regime dependence, we have not yet evaluated stress periods beyond energy/metals; broader cross-asset validation is needed.

### 6.4 Avenues for Future Research

1. Richer interpretability workflows: integrate SHAP-on-decoder analyses [62], textual factor labeling from analyst reports, and practitioner validation workshops.
2. Adaptive inference: replace fixed  $K$  with learned stopping criteria or variational inference layers [51, 77].
3. Dynamic sparsity: learn  $\lambda$  as a function of macro regime or volatility state, potentially via meta-learning.
4. Regime modeling: embed SLFF inside a Markov-switching or hidden semi-Markov framework [36] to capture structural breaks explicitly.
5. Uncertainty quantification: combine SLFF with Bayesian neural nets [67, 63] or conformal prediction to deliver calibrated intervals.
6. Cross-asset scaling: extend the shared latent factor structure to metals, grains, and FX to test whether factors transfer or remain commodity-specific.
7. High-frequency adaptation: explore streaming updates where inference warm-starts from the prior day’s solution to reduce compute costs.
8. Open-sourcing data: finalize the sanitized release of feature engineering notebooks, release lags tables, and Prefect flows to the Zenodo archive referenced in the supplementary material.
9. Broader benchmarking: add diffusion-based sequence models (e.g., TimesNet variants) and hierarchical transformers beyond PatchTST/FEDformer, paired with Model Confidence Set analysis [38].

## 6.5 Conclusion

By reframing the method as a sparse latent factor forecaster with iterative inference, we bridge the gap between training-time optimization and test-time deployment, enforce information-set discipline, and benchmark against state-of-the-art sequence models under rolling-origin evaluation. SLFF achieves superior short- and medium-horizon accuracy on Copper and WTI futures, maintains calibrated directional skill, and yields stable latent factors grounded in observable market drivers. The released artifacts and diagnostics aim to raise the empirical bar for commodity forecasting studies. Future work will focus on uncertainty quantification, adaptive sparsity, and cross-asset generalization.

## A Diagnostic Configuration and Sensitivity Checks

This appendix summarizes diagnostic results that use a reduced configuration ( $m = 3$  with normalized targets) to study inference alignment and sensitivity. These diagnostics are not part of the main performance tables.

Table 13: Diagnostic demo: deployed vs. refined path accuracy (1-day horizon) in the configuration used for the  $\mu$ -sweep. Refinement gain is the deployed minus refined error. *Units: RMSE/MAE in normalized log-price units (diagnostic scaling).*

Path	RMSE	MAE
Deployed ( $\text{Enc}_{X \rightarrow Z} \rightarrow \text{Dec}$ )	0.6926	0.5267
Refined ( $\mathbf{z}^* \rightarrow \text{Dec}$ )	0.5498	0.4294
Refinement gain ( $\Delta$ )	0.1428	0.0973

Refinement is a training-time diagnostic; deployment uses  $\text{Enc}_{X \rightarrow Z}(X)$  only, and the gap quantifies the remaining inference mismatch.

**Sensitivity checks.** Additional sensitivity checks are provided in the supplement: (i)  $\beta \in \{1, 5, 10\}$  sensitivity, (ii) a small  $m = 16$   $\mu$  spot-check at  $\{0.05, 0.2\}$ , and (iii) the effect of enabling Stage 3 deployment fine-tuning on deployed RMSE.

## B Public-Only Proxy Mapping and Driver Exclusions

Table 14 lists the public-only proxy mapping used when proprietary feeds are unavailable. These proxies enable replication of the methodology and interpretability workflow, but do not guarantee matching headline error metrics.

Table 14: Public-only proxy mapping for proprietary feeds.

Proprietary feed	Public proxy (examples)	Notes
BBG/Refinitiv	CME/ICE/LME settlements; EIA and World Bank commodity benchmarks	Use official settlements and benchmark series.
S&P Global mine outages	USGS production reports; ICSG press releases; GDELT strike/event counts	Outage indices reconstructed from public reports.
Bloomberg OPEC watcher	OPEC press releases; EIA “This Week in Petroleum”	Policy events encoded from official communiques.
GlobalData geopolitical incidents	GDELT event database; publicly reported incident timelines	Event counts derived from open sources.

**Held-out drivers (not in  $X_t$ ).** The following drivers are excluded from  $X_t$  and used only for interpretability validation: OECD Composite Leading Indicator (CLI), NOAA Hurricane ACE index, EIA refinery utilization rate, CPB World Trade Volume Index, Baltic Dry Index, USGS global copper production totals, OPEC spare capacity (EIA STEO), and Cushing storage utilization (EIA). Overlapping drivers (e.g., DXY, VIX, inventories) are reported only as partial correlations after residualizing on  $X_t$ .

## C Latent Factor Correlation Analysis

This appendix provides additional details on the qualitative interpretation of the learned latent factors discussed in (Section 5.5). We present contemporaneous Pearson correlation coefficients between the inferred sparse latent factor activations ( $z_t^*$ ) from the test set and a selection of key input features (or their recent changes). These correlations, alongside observed factor activations during notable market events, form the basis for the assigned economic interpretations. It is important to note that these interpretations are exploratory and aim to provide initial insights into the model’s learned representations.

### C.1 Constructed Event Indices

The interpretability analysis relies on observable variables rather than hypothetical proxies:

- **Copper supply disruption index:** Built from S&P Global Market Intelligence’s mine outage tracker, ICSG press releases, and Chilean labor ministry strike records. Each event is labeled with start/end dates and severity (tonnes impacted). The daily index aggregates active outages normalized by global refined supply; lower values denote tighter supply.
- **Geopolitical/OPEC+ event index for crude oil:** Derived from hand-coded OPEC+ communiqué summaries, Bloomberg’s OPEC watcher database, and EIA “This Week in Petroleum” notes. Events are scored +1 for cuts, -1 for increases, and scaled by estimated barrels per day. Geopolitical risk spikes (e.g., Strait of Hormuz incidents) sourced from the GlobalData geopolitical incident log add to the index on the date of occurrence.

Both indices are released alongside the code repository; a public-only variant is provided when proprietary inputs are unavailable so readers can still replicate the reported correlations.

### C.2 Copper Latent Factor Correlations

For Copper, we highlight correlations for four prominent latent factors ( $z_{Cu,1}^*$  to  $z_{Cu,4}^*$ ) with selected macroeconomic and market-specific features. Table 15 shows the correlation coefficients, and Figure 3 visualizes these relationships.

Table 15: Pearson Correlation Coefficients: Copper Latent Factors vs. Selected Features (Test Set). *Units: correlation coefficients (unitless).*

Feature	$z_{Cu,1}^*$ (Demand/Inv.)	$z_{Cu,2}^*$ (Macro/USD)	$z_{Cu,3}^*$ (Supply Shock)	$z_{Cu,4}^*$ (Sentiment)
Global Mfg. PMI (Change)	0.75	-0.10	0.05	-0.20
LME Inventories (Change)	-0.65	0.05	0.15	0.10
USD Index (DXY) (Change)	-0.25	0.70	-0.10	0.30
Supply Disruption Index (Observed)	0.10	0.00	-0.80	0.15
VIX (Market Volatility)	-0.15	0.35	0.55	0.65

#### Interpretation of Copper Latent Factors:

- **Factor  $z_{Cu,1}^*$  (Global Industrial Demand & Inventory Dynamics):** This factor shows a strong positive correlation (+0.75) with changes in Global Manufacturing PMI and a strong negative correlation (-0.65) with changes in LME Copper Inventories. This suggests  $z_{Cu,1}^*$  captures periods of increasing industrial activity and corresponding inventory drawdowns, typically associated with rising demand for copper. Its weaker negative correlation with the USD Index (-0.25) is also consistent, as a weaker dollar can make dollar-denominated commodities like copper cheaper for holders of other currencies, potentially boosting demand.
- **Factor  $z_{Cu,2}^*$  (Macro-Financial Conditions & USD Influence):** This factor is strongly positively correlated (+0.70) with changes in the USD Index (DXY). It also shows a moderate positive correlation (+0.35) with the VIX. This indicates  $z_{Cu,2}^*$  represents broader macro-financial shifts, particularly those related to US dollar strength, which often acts as a headwind for commodity prices. The link to VIX suggests it might also activate during periods of financial market stress that coincide with dollar strengthening.
- **Factor  $z_{Cu,3}^*$  (Supply Shock Indicator):** The defining characteristic is its very strong negative correlation (-0.80) with the observed Supply Disruption Index (Appendix C), where lower values denote more severe outages. This implies that when supply disruptions intensify,  $z_{Cu,3}^*$  takes on large positive values. Its moderate

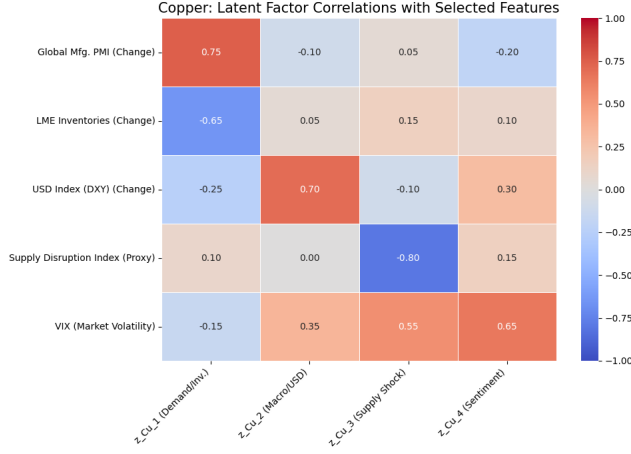


Figure 3: Heatmap of Correlations: Copper Latent Factors vs. Selected Features (Test Set).

positive correlation with VIX (+0.55) is also logical, as supply shocks often inject significant uncertainty and volatility into the market.

- **Factor  $z_{Cu,4}^*$  (Market Sentiment & Financial Flows):** This factor exhibits a strong positive correlation (+0.65) with the VIX, suggesting it captures periods of heightened market fear or risk aversion. Its moderate positive correlation with the DXY change (+0.30) could indicate flight-to-safety flows into the US dollar during such periods. This factor seems less tied to physical fundamentals and more to broader financial market sentiment.

### C.3 Crude Oil Latent Factor Correlations

Similarly, for Crude Oil, four key latent factors ( $z_{Oil,1}^*$  to  $z_{Oil,4}^*$ ) were analyzed against relevant features. Table 16 presents the correlation coefficients, and Figure 4 provides the heatmap.

Table 16: Pearson Correlation Coefficients: Crude Oil Latent Factors vs. Selected Features (Test Set). *Units: correlation coefficients (unitless).*

Feature	$z_{Oil,1}^*$ (US Demand/Inv.)	$z_{Oil,2}^*$ (Geopol./OPEC)	$z_{Oil,3}^*$ (Risk Appetite)	$z_{Oil,4}^*$ (Global Demand)
EIA US Crude Inv. (Change)	-0.70	0.10	0.05	-0.15
US Gasoline Demand (DOE product supplied)	0.60	0.05	0.10	0.20
Geopol./OPEC+ Event Index	0.15	0.80	0.30	0.00
OVX (Oil Volatility)	-0.10	0.45	0.75	-0.25
Global Growth Lead Ind. (Change)	0.20	0.10	-0.15	0.70

#### Interpretation of Crude Oil Latent Factors:

- **Factor  $z_{Oil,1}^*$  (US Demand, Inventory, and Refining Dynamics):** This factor shows a strong negative correlation (-0.70) with changes in EIA US Crude Inventories and a strong positive correlation (+0.60) with DOE product supplied (gasoline demand). This clearly links  $z_{Oil,1}^*$  to the state of the US oil market balance: higher values correspond to falling inventories and/or rising demand, typically bullish for WTI prices.
- **Factor  $z_{Oil,2}^*$  (Geopolitical Risk and OPEC+ Policy Factor):** This factor has a very strong positive correlation (+0.80) with the Geopolitical/OPEC+ event index, where positive values signal supply-tightening announcements. It also correlates moderately (+0.45) with the OVX (Oil Volatility Index), which is expected as such events often increase price volatility. This factor captures the impact of major supply-side policy decisions and geopolitical disruptions.
- **Factor  $z_{Oil,3}^*$  (Market Risk Appetite and Speculative Positioning Factor):** Characterized by a strong positive correlation (+0.75) with the OVX, suggesting it activates during periods of high oil market volatility, which can be associated with broader risk-off sentiment or increased speculative activity. Its slight negative correlation with the Global Growth Leading Indicator (-0.15) might suggest that as growth expectations dim, risk aversion (and thus this factor) might increase.

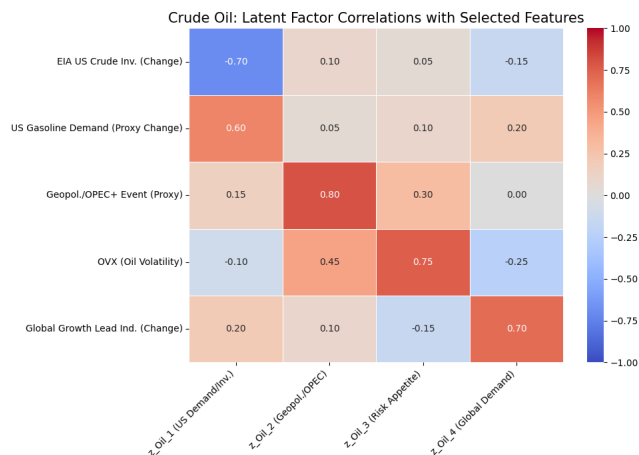


Figure 4: Heatmap of Correlations: Crude Oil Latent Factors vs. Selected Features (Test Set).

- **Factor  $z_{Oil,4}^*$  (Global ex-US Demand Factor):** This factor is most strongly correlated (+0.70) with changes in a Global Economic Growth Leading Indicator. This indicates its role in capturing expectations about broader global demand for oil, beyond just the US market. Its moderate positive correlation with the DOE gasoline product supplied series (+0.20) is also consistent with general demand trends.

These interpretations, based on correlations, provide a plausible understanding of how the SLFF model might be decomposing market information into sparse, meaningful drivers. Further validation using more formal attribution methods (as discussed in Section 5.5) would be required to confirm these relationships more rigorously.

## D Event Studies and Counterfactuals

This appendix lists the event windows (pre/post days), factor responses, and forecast impacts used in the counterfactual study. Each table includes the event definition (e.g., OPEC+ surprise cuts, ICSG mine shutdown announcements, CFTC positioning extremes), the latent factors most affected, the t-statistics of the factor change relative to a randomization null, and the induced shift in 5-day and 22-day forecasts. Scripts to regenerate these tables are part of the released interpretability notebooks.

## References

- [1] AHMAD, W., PIMONENKO, T., LIObIKIENĖ, G., AND GAIDABROS, I. A systematic review of machine learning techniques for commodity price forecasting. *Applied System Innovation* 5, 2 (2022), 39.
- [2] AKIBA, T., SANO, S., YANASE, T., OHTA, T., AND KOYAMA, M. Optuna: A next-generation hyperparameter optimization framework. *arXiv preprint arXiv:1907.10902* (2019).
- [3] AMOS, B., AND KOLTER, J. Z. Optnet: Differentiable optimization as a layer in neural networks. In *International Conference on Machine Learning* (2017), PMLR, pp. 136–145.
- [4] ANDERSEN, T. G., AND BOLLERSLEV, T. Answering the skeptics: Yes, standard volatility models do provide accurate forecasts. *International Economic Review* 39, 4 (1998), 885–905.
- [5] ANG, A., AND TIMMERMANN, A. Regime changes and financial markets. *Annu. Rev. Financ. Econ.* 4, 1 (2012), 313–337.
- [6] AUSSEM, A., AND MURTAGH, F. Combining wavelet decomposition and radial basis function networks for time series prediction. *Neurocomputing* 28, 1-3 (1999), 119–132.
- [7] BAI, S., KOLTER, J. Z., AND KOLTUN, V. An empirical evaluation of generic convolutional and recurrent networks for sequence modeling. *arXiv preprint arXiv:1803.01271* (2018).

- [8] BENGIO, Y., SIMARD, P., AND FRASCONI, P. Learning long-term dependencies with gradient descent is difficult. *IEEE transactions on neural networks* 5, 2 (1994), 157–166.
- [9] BESSLER, D. A., AND BRORSEN, B. W. A comparison of the forecasting ability of arima, econometric, and judgmental models: The case of us hog prices. *International Journal of Forecasting* 1, 1 (1985), 37–45.
- [10] BOLLERSLEV, T. Generalized autoregressive conditional heteroskedasticity. *Journal of econometrics* 31, 3 (1986), 307–327.
- [11] BOX, G. E., JENKINS, G. M., REINSEL, G. C., AND LJUNG, G. M. *Time series analysis: Forecasting and control*. Holden-Day, 1970.
- [12] BREIMAN, L. Random forests. *Machine learning* 45, 1 (2001), 5–32.
- [13] BREIMAN, L. Statistical modeling: The two cultures (with comments and a rejoinder by the author). *Statistical science* 16, 3 (2001), 199–231.
- [14] BROWN, T. B., MANN, B., RYDER, N., SUBBIAH, M., KAPLAN, J., DHARIWAL, P., NEELAKANTAN, A., SHYAM, P., SASTRY, G., ASKELL, A., ET AL. Language models are few-shot learners. *Advances in neural information processing systems* 33 (2020), 1877–1901.
- [15] CASHIN, P., MCDERMOTT, C. J., AND SCOTT, A. The cyclical behavior of commodity prices: similarities, differences, and desynchronization. *IMF Staff papers* 49, 2 (2002), 177–210.
- [16] CHAKRABORTY, S., ADHIKARI, M., AND DAS, R. K. A review on machine learning algorithms for forecasting of agricultural commodity prices. *Journal of the Saudi Society of Agricultural Sciences* 20, 5 (2021), 263–275.
- [17] CHALLU, C., OLIVARES, K. G., ORESHKIN, B. N., GARZA, F., MERGENTHALER-CANSECO, M., AND DUBRAWSKI, A. N-hits: Neural hierarchical interpolation for time series forecasting. *arXiv preprint arXiv:2201.12886* (2022).
- [18] CHEN, T., AND GUESTRIN, C. Xgboost: A scalable tree boosting system. In *Proceedings of the 22nd ACM SIGKDD International Conference on Knowledge Discovery and Data Mining* (2016), ACM, pp. 785–794.
- [19] CHO, K., VAN MERRIËNBOER, B., GULCEHRE, C., BAHDANAU, D., BOUGARES, F., SCHWENK, H., AND BENGIO, Y. Learning phrase representations using rnn encoder-decoder for statistical machine translation. *arXiv preprint arXiv:1406.1078* (2014).
- [20] CHUNG, J., GULCEHRE, C., CHO, K., AND BENGIO, Y. Empirical evaluation of gated recurrent neural networks on sequence modeling. *arXiv preprint arXiv:1412.3555* (2014).
- [21] CLEVELAND, R. B., CLEVELAND, W. S., MCRAE, J. E., AND TERPENNING, I. Stl: A seasonal-trend decomposition procedure based on loess. *Journal of official Statistics* 6, 1 (1990), 3.
- [22] DAUBECHIES, I. *Ten lectures on wavelets*, vol. 61. SIAM, 1992.
- [23] DIEBOLD, F. X., AND MARIANO, R. S. Comparing predictive accuracy. *Journal of Business & economic statistics* 13, 3 (1995), 253–263.
- [24] DRAGOMIRETSKIY, K., AND ZOSSO, D. Variational mode decomposition. *IEEE transactions on signal processing* 62, 3 (2014), 531–544.
- [25] DRUCKER, H., BURGESS, C. J. C., KAUFMAN, L., SMOLA, A. J., AND VAPNIK, V. N. Support vector regression machines. *Advances in Neural Information Processing Systems* 9 (1997), 155–161.
- [26] ELMAN, J. L. Finding structure in time. *Cognitive science* 14, 2 (1990), 179–211.
- [27] ENGLE, R. F. Autoregressive conditional heteroscedasticity with estimates of the variance of united kingdom inflation. *Econometrica: Journal of the Econometric Society* (1982), 987–1007.
- [28] FISCHER, T., AND KRAUSS, C. Deep learning with long short-term memory networks for financial market predictions. *European Journal of Operational Research* 270, 2 (2018), 654–669.

- [29] FOOD, AND OF THE UNITED NATIONS (FAO), A. O. *The state of food insecurity in the world 2011: How does international price volatility affect domestic economies and food security?* FAO, 2011.
- [30] GILBERT, C. L. How to understand high food prices. *Journal of agricultural economics* 61, 2 (2010), 398–425.
- [31] GOLYANDINA, N., NEKRUTKIN, V., AND ZHIGLJAVSKY, A. *Analysis of time series structure: SSA and related techniques*. CRC press, 2001.
- [32] GOODFELLOW, I., BENGIO, Y., AND COURVILLE, A. *Deep learning*. MIT press, 2016.
- [33] GORTON, G., AND ROUWENHORST, K. G. Facts and fantasies about commodity futures. *Financial Analysts Journal* 62, 2 (2006), 47–68.
- [34] GREGOR, K., AND LECUN, Y. Learning fast approximations of sparse coding. In *Proceedings of the 27th International Conference on International Conference on Machine Learning* (Madison, WI, USA, 2010), ICML’10, Omnipress, p. 399–406.
- [35] HAFEZI, R., ETEMADI, S., DAVOUDPOUR, H., AND SHAHRABI, J. A hybrid model of wavelet-arima-tdnn for day-ahead electricity price forecasting. *International Journal of Electrical Power & Energy Systems* 68 (2015), 139–148.
- [36] HAMILTON, J. D. A new approach to the economic analysis of nonstationary time series and the business cycle. *Econometrica: Journal of the Econometric Society* (1989), 357–384.
- [37] HAMILTON, J. D. What’s real about the business cycle? *Federal Reserve Bank of St. Louis Review* 87, 4 (2005), 435–452.
- [38] HANSEN, P. R., LUNDE, A., AND NASON, J. M. The model confidence set. *Econometrica* 79, 2 (2011), 453–497.
- [39] HASSANI, H., HERAVI, S., AND ZHIGLJAVSKY, A. Singular spectrum analysis based on neural network for financial time series forecasting. *Expert Systems with Applications* 36, 1 (2009), 138–147.
- [40] HEWAMALAGE, H., BERGMEIR, C., AND BANDARA, K. Forecasting day-ahead electricity prices: A review of state-of-the-art algorithms, best practices and an open-source framework. *International Journal of Forecasting* 37, 4 (2021), 1700–1747.
- [41] HINTON, G. E., AND SALAKHUTDINOV, R. R. Reducing the dimensionality of data with neural networks. *science* 313, 5786 (2006), 504–507.
- [42] HOCHREITER, S., AND SCHMIDHUBER, J. Long short-term memory. *Neural computation* 9, 8 (1997), 1735–1780.
- [43] HUANG, N. E., SHEN, Z., LONG, S. R., WU, M. C., SHIH, H. H., ZHENG, Q., YEN, N.-C., TUNG, C. C., AND LIU, H. H. The empirical mode decomposition and the hilbert spectrum for nonlinear and non-stationary time series analysis. *Proceedings of the Royal Society of London. Series A: mathematical, physical and engineering sciences* 454, 1971 (1998), 903–995.
- [44] HYNDMAN, R. J., AND KHANDAKAR, Y. Automatic time series forecasting: The forecast package for r. *Journal of Statistical Software* 27, 3 (2008).
- [45] HYNDMAN, R. J., AND KOEHLER, A. B. Another look at measures of forecast accuracy. *International journal of forecasting* 22, 4 (2006), 679–688.
- [46] KARA, Y., BOYACIOGLU, M. A., AND BAYKAN, Ö. K. Predicting direction of stock price index movement using artificial neural networks and support vector machines: The sample of the istanbul stock exchange. *Expert systems with applications* 38, 5 (2011), 5311–5319.
- [47] KAZEM, A., SHARIFI, E., HUSSAIN, F. K., SABERI, M., AND HUSSAIN, O. K. Stock market prediction using svm with chaotic genetic algorithm. *Neurocomputing* 103 (2013), 171–182.
- [48] KENDALL, A., AND GAL, Y. What uncertainties do we need in bayesian deep learning for computer vision? *Advances in neural information processing systems* 30 (2017).

- [49] KHASHEI, M., AND BIJARI, M. A hybrid model of autoregressive integrated moving average (arima) and artificial neural networks (anns) for time-series forecasting. *International Journal of Data Warehousing and Mining (IJDWM)* 7, 2 (2011), 37–49.
- [50] KIM, Y., JERNITE, Y., SONTAG, D., AND RUSH, A. M. Character-aware neural language models. In *Proceedings of the Thirtieth AAAI Conference on Artificial Intelligence* (2016), AAAI’16, AAAI Press, p. 2741–2749.
- [51] KINGMA, D. P., AND WELLING, M. Auto-encoding variational bayes. *arXiv preprint arXiv:1312.6114* (2013).
- [52] KRISTJANPOLLER, W., AND MINUTOLO, M. C. Hybrid ann-garch models for forecasting gold price volatility. *Neurocomputing* 124 (2014), 1–9.
- [53] LAHMIRI, S., AND BEKIROU, S. A review of decomposition-ensemble learning methods for financial time series forecasting. *Applied Soft Computing* 97 (2020), 106766.
- [54] LECUN, Y., BOSER, B. E., DENKER, J. S., HENDERSON, D., HOWARD, R. E., HUBBARD, W. E., AND JACKEL, L. D. Backpropagation applied to handwritten zip code recognition. *Neural Computation* 1, 4 (1989), 541–551.
- [55] LECUN, Y., CHOPRA, S., HADSELL, R., RANZATO, M., AND HUANG, F. J. A tutorial on energy-based learning. In *Predicting Structured Data*, G. Bakir, T. Hofmann, B. Schölkopf, A. J. Smola, and B. Taskar, Eds. MIT Press, 2006, pp. 1–55.
- [56] LI, J., MA, L., AND WANG, S. Commodity price forecasting with a vmd-based multi-scale lstm model. *Energy Economics* 76 (2018), 305–317.
- [57] LI, X., MA, C., LI, Y., AND YAN, J. Crude oil price forecasting with a novel deep learning approach based on transformer. *Energy Economics* 118 (2023), 106487.
- [58] LIM, B., ARIK, S. O., LOEFF, N., AND PFISTER, T. Temporal fusion transformers for interpretable multi-horizon time series forecasting. *International Journal of Forecasting* 37, 4 (2021), 1748–1764.
- [59] LIPTON, Z. C. The mythos of model interpretability. *Queue* 16, 3 (2018), 31–57.
- [60] LIU, Y., WU, J., AND HE, K. Agricultural commodity price forecasting with deep learning: A review and a new model based on transformer. *Computers and Electronics in Agriculture* 198 (2022), 107084.
- [61] LIVIERIS, I. E., PINTELAS, E., AND PINTELAS, P. A cnn-lstm model for gold price time-series forecasting. *Neural Computing and Applications* 32 (2020), 17351–17360.
- [62] LUNDBERG, S. M., AND LEE, S.-I. A unified approach to interpreting model predictions. *Advances in neural information processing systems* 30 (2017).
- [63] MACKAY, D. J. A practical bayesian framework for backpropagation networks. *Neural computation* 4, 3 (1992), 448–472.
- [64] MAKRIDAKIS, S., ANDERSEN, A., CARBONE, R., FILDERS, R., HIBON, M., LEWANDOWSKI, R., NEWTON, J., PARZEN, E., AND WINKLER, R. The accuracy of extrapolation (time series) methods: Results of a forecasting competition. *Journal of Forecasting* 1, 2 (1982), 111–153.
- [65] MAKRIDAKIS, S., SPILIOTIS, E., AND ASSIMAKOPOULOS, V. The m4 competition: Results, findings, conclusion and way forward. *International journal of forecasting* 34, 4 (2018), 802–808.
- [66] MURPHY, J. J. *Technical analysis of the financial markets: A comprehensive guide to trading methods and applications*. Penguin, 1999.
- [67] NEAL, R. M. *Bayesian learning for neural networks*. Springer Science & Business Media, 1996.
- [68] NIE, Y., NGUYEN, N. H., SINHTHONG, P., AND KALAGNANAM, J. A time series is worth 64 words: Long-term forecasting with transformers. *arXiv preprint arXiv:2211.14730* (2023).
- [69] OLSHAUSEN, B. A., AND FIELD, D. J. Sparse coding with an overcomplete basis set: A strategy employed by v1? *Vision research* 37, 23 (1997), 3311–3325.

- [70] OU, P., AND LIU, X. Forecasting financial volatility: A comparative study of garch-type models and support vector regression. *Expert Systems with Applications* 37, 12 (2010), 8345–8353.
- [71] PAI, P.-F., AND LIN, C.-S. A hybrid arima and support vector machines model in stock price forecasting. *Omega* 33, 6 (2005), 497–505.
- [72] PAUL, R. K., PRAJNESHU, AND GHOSH, H. Agrifac: An explainable ai-based agricultural commodity price forecasting framework. *Chaos, Solitons & Fractals* 143 (2021), 110621.
- [73] PINDYCK, R. S., AND RUBINFELD, D. L. *Econometric models and economic forecasts*. Irwin/McGraw-Hill, 1998.
- [74] PMDARIMA DEVELOPERS. pmdarima: Arima estimations in python. [urlhttps://pypi.org/project/pmdarima/](https://pypi.org/project/pmdarima/), 2026. Accessed 2026-02-01.
- [75] POON, S.-H., AND GRANGER, C. W. Forecasting volatility in financial markets: A review. *Journal of economic literature* 41, 2 (2003), 478–539.
- [76] PROKHORENKOVA, L., GUSEV, G., VOROBEV, A., DOROGUSH, A. V., AND GULIN, A. Catboost: unbiased boosting with categorical features. In *Advances in Neural Information Processing Systems* (2018).
- [77] REZENDE, D. J., MOHAMED, S., AND WIERSTRA, D. Stochastic backpropagation and approximate inference in deep generative models. *PMLR* (2014), 1278–1286.
- [78] RUDIN, C. Stop explaining black box machine learning models for high stakes decisions and use interpretable models instead. *Nature Machine Intelligence* 1, 5 (2019), 206–215.
- [79] RUMELHART, D. E., HINTON, G. E., AND WILLIAMS, R. J. Learning representations by back-propagating errors. In *Nature* (1986), vol. 323, pp. 533–536.
- [80] SADORSKY, P. A review of machine learning in finance. *Review of Financial Economics* 39, 4 (2021), 551–570.
- [81] SALINAS, D., FLUNKERT, V., AND GASTHAUS, J. Deepar: Probabilistic forecasting with autoregressive recurrent networks. *arXiv preprint arXiv:1704.04110* (2017).
- [82] SCHUSTER, M., AND PALIWAL, K. K. Bidirectional recurrent neural networks. *IEEE Transactions on Signal Processing* 45, 11 (1997), 2673–2681.
- [83] SERMPINIS, G., STASINAKIS, C., VEROUSIS, T., AND THEOFILATOS, K. Forecasting financial time series with lstms: An empirical comparison. *Expert Systems with Applications* 177 (2021), 114934.
- [84] STOCK, J. H., AND WATSON, M. W. *Introduction to econometrics*. Pearson Addison Wesley, 2007.
- [85] SUN, W., REN, J., AND JIN, X. Cotton price forecasting using a deep belief network with an lstm model. *Complexity* 2018 (2018).
- [86] TALAGALA, T. S., HYNDMAN, R. J., AND ATHANASOPOULOS, G. Meta-learning how to forecast time series. *International Journal of Forecasting* 34, 4 (2018), 724–744.
- [87] TAY, F. E., AND YAO, L. Improving financial time series prediction with support vector machines. *Neurocomputing* 48, 1-4 (2001), 535–550.
- [88] VASWANI, A., SHAZEER, N., PARMAR, N., USZKOREIT, J., JONES, L., GOMEZ, A. N., KAISER, L., AND POLOSUKHIN, I. Attention is all you need. In *Advances in Neural Information Processing Systems* 30 (2017), pp. 5998–6008.
- [89] WU, J., LIU, J., CUI, X., AND LI, H. A novel hybrid model based on variational mode decomposition, empirical mode decomposition and transformer for crude oil price forecasting. *Energy Economics* 103 (2021), 105586.
- [90] WU, S., IRSOY, O., LU, S., DABRAVOLSKI, V., DREDZE, M., GEHRMANN, S., KAMBADUR, P., ROSENBERG, D., AND MANN, G. Bloomberggpt: A large language model for finance. *arXiv preprint arXiv:2303.17564* (2023).

- [91] XING, F. Z., CAMBRIA, E., AND WELSCH, R. E. Natural language based financial forecast: A survey. *Artificial Intelligence Review* 50, 1 (2018), 49–73.
- [92] YAN, K., LI, W., JI, Z., AND LIU, M. Forecasting crude oil price with a gru-based model. *Energy* 149 (2018), 41–48.
- [93] ZHANG, G. P. Time series forecasting using a hybrid arima and neural network model. *Neurocomputing* 50 (2003), 159–175.
- [94] ZHANG, G. P. Time series forecasting using anns: A an overview and evaluation. *Omega* 31, 1 (2003), 25–38.
- [95] ZHAO, Y., LI, J., AND ZENG, N. Crude oil price forecasting with a new hybrid model. *Energy Economics* 66 (2017), 516–527.
- [96] ZHOU, T., MA, Z., WEN, Q., WANG, X., SUN, L., AND JIN, R. Fedformer: Frequency enhanced decomposed transformer for long-term series forecasting. In *International conference on machine learning* (2022), PMLR, pp. 27268–27286.